

Carton dataset synthesis based on foreground texture replacement

Lijun Gou^a, Shengkai Wu^a, Jinrong Yang^a, Hangcheng Yu^a, Linchen Xi^a, Xiaoping Li^{a,*}, Chao Deng^a

^aState Key Laboratory of Digital Manufacturing Equipment and Technology, Huazhong University of Science and Technology, Wuhan, 430074, China.

Abstract

One major impediment in rapidly deploying object detection models for industrial applications is the lack of large annotated datasets. Currently, in the e-commerce logistics industry, there is a Sacked Carton Dataset(SCD) that contains carton images from three scenarios such as comprehensive pharmaceutical logistics company(CPLC), e-commerce logistics company(ECLC), fruit market(FM). However, due to domain shift, the model trained with carton datasets from one of the three scenarios in SCD has poor generalization ability when applied to the rest scenarios. To solve this problem, a novel image synthesis method is proposed to replace the foreground texture of the source datasets with the foreground instance texture of the target datasets. This method can greatly augment the target datasets and improve the model's performance. We firstly propose a surfaces segmentation algorithm to identify the different surfaces of the carton instance. Secondly, a contour reconstruction algorithm is proposed to solve the problem of occlusion, truncation, and incomplete contour of carton instances. Finally, we use the Gaussian fusion algorithm to fuse the background from the source datasets with the foreground from the target datasets. In the experiments, our novel image synthesis method can largely boost AP by at least 4.3% ~ 6.5% on RetinaNet and 3.4% ~ 6.8% on Faster R-CNN for the target domain. And on the source domain, the performance AP can be improved by 1.7% ~ 2% on RetinaNet and 0.9% ~ 1.5% on Faster R-CNN. Code is available [here](#).

Keywords: domain shift, surfaces segmentation, dataset synthesis, data augmentation

1. Introduction

In the past few years, Convolutional Neural Networks (CNN) have significantly prompted the development of many computer vision tasks [1, 2, 3, 4, 5, 6]. However, the training of such models [1, 2, 3, 4, 5, 6] with millions of parameters requires a massive amount of labeled training data, such as MS COCO[7], CityScapes[8] and ImageNet[9] to achieve state-of-the-art results. At the same time, traditional object detection model is designed based on the condition of independent identically distributed. However, due to the changing of scene, light, imaging angle and instance texture, object detection model do not satisfy the condition. It is obvious that the creation of such massive datasets has become one of the main limitations of these approaches, the datasets need to be accurately annotated, and are very expensive, time-consuming, and error-prone.

With the development of the e-commerce logistics industry, logistics transfer is becoming busier and busier. The efficiency about the goods in and out of the warehouse is more and more important

*Corresponding author

Email addresses: getglj@hust.edu.cn (Lijun Gou), lixiaoping@hust.edu.cn (Xiaoping Li)



Figure 1: Intelligent robot for automatic loading and unloading, the first robot is Parcel Robot from Germany, the second robot is PIQR from Netherlands, the last is ours robot.

for the logistics transfer. This promote the development of automatic loading and unloading intelligent robots as shown in Figure.1. One of the most critical techniques for these intelligent robots is the detection of dense cartons. We have built a carton dataset SCD[10] for carton detection, but the goods are diverse in different spots. So the carton datasets from different scenes are inconsistent in carton logo, color, texture, etc as shown in Figure.2, which means detectors trained by SCD can not satisfy the assumption of independent and identical distribution.

To tackle the above issue, many researchers resort to data augmentation strategies to increase data coverage by utilizing available training data. Common data augmentation methods include random cropping, color jittering, random deformation, etc. However, these methods can only introduce limited data variation, so they improve the performance slightly. Recently, several works[11, 12, 13] propose crop-and-paste data augmentation schemes for object detection [3, 5, 6], which is cropping some object foregrounds and pasting them into the target scene. However, these methods need to collect lots of object foregrounds with different poses, it is expensive and time-consuming. And the combination relationship of object foregrounds and backgrounds is complex. As a result, the augmentation samples may look unrealistic and hinder the model learning.

Here, we propose a novel dataset synthesis method of replacing the foreground instance texture with the instance texture from the new scene to augment the datasets, the augmentation samples may look more realistic. And it is convenient to compare with the methods in Ref.[11, 12, 13], because our method do not need to collect variety of pictures for each kind of carton with different poses. As shown in Fig.3, our method involves four key stages:(1) labeled the images with our rules; (2) segment different surfaces of the carton to realize texture decoupling; (3) because the contour of the instance texture from target scene is complete, we construct a complete contour for the surface of the carton; (4) synthesize images with Gaussian fusion method. We perform foreground instance texture replacement in CPLC scene, and all experiments are verified and tested on models including Faster R-CNN[3] and RetinaNet[6].

Our method has three main contributions: (1) we propose a novel dataset synthesis method of replacing the foreground instance texture to generate the target dataset with the high homogeneity of the carton palletizing form as shown in Figure 2; (2) We propose a surfaces segmentation algorithm for texture decoupling. (3) We propose a contour reconstruction algorithm based on the parallelogram rule to reconstruct the incomplete contours.



Figure 2: (a) The images come from a comprehensive pharmaceutical logistics company(CPLC); (b) The images come from an e-commerce logistics company(ECLC); (c) The images come from a fruit market(FM); (d) The foreground texture dataset from FM. In the figure (a), (b) , (c), the stacking and palletizing structures of all cartons are similar in all scenarios.

2. Related Work

2.1. Object detection

In the past few years, with the development of Convolutional Neural Networks, object detection has been applied in many scenes, such as security, autonomous driving, defect detection. The CNN-based detection models are mainly classified into the single-stage detectors[6, 14, 5, 4, 15] and two-stage detectors[3, 16, 17]. Faster R-CNN[3], acted as the mainstream two-stage detector, firstly uses RPN to generate region proposals which are fed into the FPN to conduct accurate localization and classification tasks. And some works such as Cascade R-CNN[18], Libra R-CNN[19], Mask R-CNN[20] have inspired by Faster R-CNN. Although the two-stage detection models can achieve considerable performance, its efficiency is poor because of the complex multi-stage processing. To solve the problem, researchers have proposed many single-stage detection models such as YOLO[21], YOLO V4[4], SSD[5] and RetinaNet[6]. SSD[5] not only draws on the idea of RPN[3] but also adopts feature pyramid to detect multi-scale objects. Recently, RetinaNet[6] proposed the focal loss to solve the imbalance problem between the easy examples and hard examples. Our paper uses RetinaNet[6] and Faster R-CNN[3] as the baselines to demonstrate the effectiveness of our method.

2.2. Data Augmentations

Data augmentations have played an key role in achieving state-of-the-art results for many computer vision tasks such as image classification[1, 22] on ImageNet[23], object detection[3, 6, 5] on MS COCO[7]. And the simplest strategy for solving overfitting problem is to train CNN-based models on larger scale of data. Many data augmentation strategies have been proposed to augment the existing datasets such as random crop[23, 24], color jittering[24], Auto/RandAugment[25, 26], and random expansion[27, 5]. These augmentation strategies are originally designed for image classification[23] and are mainly used for improving the classification models' invariance to data transformations in image classification task.

2.3. Copy-Paste Augmentation

The methods based on the foreground and background decoupling and recombination is mostly used in the field of dataset expansion and dataset generation to improve the generalization of the model. For example, McLaughlin N et al.[28] proposed to extract the foreground of the target dataset and then fuse with the street background to reduce the bias of the datasets. Georgakis G et al.[29] used the depth information of the scene and combined with foreground examples to explore semantic fusion in a given background image. Dwibedi D et al.[11] used a variety of synthetic methods to ignore these subtle pixel artifacts and focus only on the object appearance during data generating. But this method has defects because it can not cover all possible synthetic methods. Tripathi S et al.[13] used adversarial learning to construct a task-driven synthesis network for foreground instance and background image synthesis. Liu S et al.[12] used the foreground instances and background images to generate pedestrian data and then cycGAN [30] is utilized for style transfer to achieve pedestrian detection in different scenes. At present, the methods of the foreground instance and background image fusion mainly focus on the contextual semantic relationship of the foreground instance and background image[28, 29, 31, 13]. In addition, these methods in Ref.[11, 12, 13, 27] focus on how to ignore these subtle pixel artifacts during the synthesis process. The difference of the method in our paper compared with the methods in Ref.[11, 12, 13, 27] is that the scale and position of instance in the background image remains unchanged. And the carton instance is composed of multiple surfaces, different combinations of the same surface can generate a new instance with different perspective and poses. Therefore, compared with the methods in Ref. [11, 12, 13, 27], our method does not need to collect a large number of foreground instances with different perspectives and poses.

3. Method

3.1. Approach overview

We propose a simple approach to rapidly collect data for target domain while requiring little time and no human annotation. And the key idea of our approach is keeping the contour of the carton from source domain unchanging to replace their foreground texture with the target texture. This approach can capture all of the visual diversity of an instance with different views, scales, and orientation. And our approach can maintain the contextual semantic relationship of the image to make the synthesized image more realistic. The architecture of our proposed carton datasets synthesis method is illustrated in Fig.3. And there are six steps of our method:

(1) **Collect source images:** We have built a Stacked Carton Dataset(SCD)[10] for carton detection task in the warehousing and logistics industry.

(2) **Labeling process:** In the image plane, the carton may contain one, two, or three visible surfaces depending on the shooting angle and each surface has different texture. According to the traditional labeling rules, different surfaces cannot be distinguished. So we have designed new labeling rules(as shown in Sec.3.2) to help surface segmentation.

(3) **Surfaces segmentation algorithm:** As shown in Fig.4, each surface of the carton is a closed polygon such as: 2-3-4-5, 4-6-7-8-5 and 1-2-5-8-9. So the problem of surface segmentation is to find all the closed polygon without any overlap. Here, we consider the labeled point as a city, so the problem can be solved by the method of TSP[32]. Our algorithm consists of three steps(see Sec.3.3 for detailed information) as shown in third module in Fig.3. The first step is data processing, the second step is calculating cost matrix as a directed graph and the third step is to get all closed polygons of the carton with TSP algorithm.

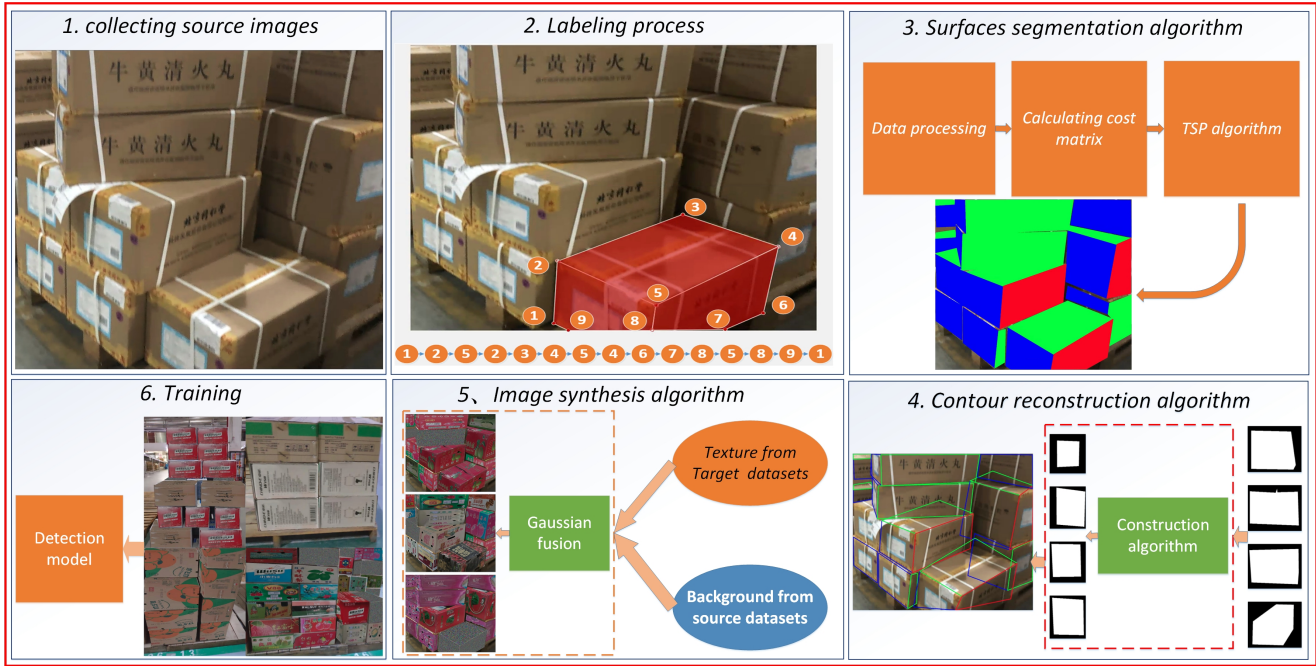


Figure 3: We propose a carton datasets synthesis method for object detection with different perspectives and poses. Firstly, we have built a Stacked Carton Datasets(SCD)[10]; secondly, we label the images with our labeling rules; thirdly, we perform surfaces segmentation algorithm to get different surfaces; then we use the contour reconstruction algorithm to construct a complete quadrilateral contour in part 4; next we use Gaussian filtering algorithm for foreground texture replacement and image synthesis; finally, we use the generated data to train the detection model.

(4) **Contour reconstruction algorithm:** The contour of the foreground texture from target datasets is complete as shown in Fig.2d. So when the contour of the surface from source datasets is incomplete, we should construct a complete contour. And we construct a parallelogram as the complete contour for the surface(see Sec.3.4 for detailed information).

(5) **Image synthesis:** We use Gaussian fusion method to generate images. And we use a random noise as negative texture example to make the detection model focus only on the object appearance(see Sec.3.5 for detailed information).

(6) **Training:** Finally, we use the generated images and the source images to train the detection models.

3.2. Labeling method

SCD[10] mainly focus on the task of carton detection in the logistics industry. The images in SCD are collected from 3 scenarios of different locations. And each scenario contains a large number of neatly stacked cartons as shown in Figure 2.

Data collection: SCD mainly collects carton images in the loading and unloading dock scenes. Because the cameras of the palletizing robots is approximately parallel to the surface of the goods, the imaging plane is approximately parallel to the surface of the goods during data collection(as shown in Figure 2). And the shooting distance is within 5 m.

Labeling rules: SCD utilizes LabelMe[33] for labeling. Besides, to help the robot pick up the goods, one auxiliary labling rule is proposed. **Occlusion/All:** it is labeled as "Occlusion" when all the surfaces of the carton are occluded, and "All" when at least one surface of the carton is not occluded. To segment different surfaces of the carton, we have designed a new labeling method as shown in Figure 4 and the **labeling rules** includes: (1) only the two-line points can be selected



Figure 4: Labeling method. The number represents labeled point and the arrows represents the labeling process. **Common lines:** the line between two visible surfaces, such as line 5-2, 5-4, 5-8. **Three-line points:** the points which are intersected by three visible lines such as point 5, 2, 4, 8; **Two-line points:** the points which are intersected by two visible lines such as point 1, 3, 6, 7, 9.

as the start points; (2) the points should be labeled in a clockwise direction; (3) the common lines should be repeatedly labeled twice.

3.3. Surfaces segmentation algorithm

Data procssing: Based on our proposed labeling method, it is easy to judge whether the point is a faceted point according to definition 1. But during labeling process, the coordinates of the same faceted points have errors when labeling according to the third labeling rule. Thus, we judge the point is the same faceted points in labeled points set P^S (as shown Figure 4) according to Eq.1(3 to 11 line in Algorithm1). Then the average of the coordinate about the same faceted points is used to replace the values of the same faceted points in P^S to get a new point set as P^{new} (17 to 18 line in Algorithm1). Finally, we get a point set P^t without repeated points from P^{new} (12 to 16 line in Algorithm1) to calculate the cost matrix.

Definition 1. The three-line points are faceted points as shown in Fig.4. According to the labeling rules in section 3.2, the points which are repeated more than 1 times in the labeled points are faceted points.

$$D(p_i, p_j) = \sqrt{(p_{i_x} - p_{j_x})^2 + (p_{i_y} - p_{j_y})^2} \leq \psi \quad (1)$$

In Eq.1, $p_i, p_j \in P^S$, and (p_{i_x}, p_{i_y}) is the coordinate of p_i . ψ is a hyperparameter to determine whether two points are the same faceted point, $\psi = 25$ in here.

Calculating cost matrix: For Traveling Salesman Problem(TSP), it is important to get a cost matrix about each city. And in our method, each labeled point is regarded as a city. So we calculate the cost matrix of each point. We suppose that the $G(P^t, V)$ is a directed graph, $V = [V_{i,j}]_{k \times k}$ is the cost matrix between each point in P^t which is calculated by Eq.2(20 to 25 line in Algorithm1). In Eq.2, the symbol \rightarrow means the index of point p_i in P^{new} plus 1 is equal to the index of p_j in P^{new} . It means that p_i to p_j is connected and assigned the value 1, otherwise it is not connected and the value is infinite represented by Inf .

$$V_{i,j} = \begin{cases} 1, p_i \rightarrow p_j \\ Inf \end{cases} \quad \text{s.t.} \begin{cases} p_i, p_j \in P^t \\ P^t \subseteq P^{new} \end{cases} \quad (2)$$

Algorithm 1: Surfaces segmentation algorithm

Input: $P^S = \{p_i\}_{i=0}^n$: the points list of the instance from labeling points;

Output: $P_{result} = \{p_i\}_{i=0}^2$: the points of surfaces in the carton;

```
1 Initialize:  $\psi = 25$ ;  $index = []$ ,  $[\dots]$ : the Array which save the indexes of points with
   same coordinate in  $P^S$ ;  $P^t = []$ : the Array which do not have repeated points.
2 #Data proccsing:
3 for  $i = 0$  to  $n$  do
4    $index[i] \leftarrow \{i\}$ 
5   for  $j = 0$  to  $n$  do
6     Calculate  $D(P^S[i], P^S[j])$  by Eq.(1)
7     if  $D(P^S[i], P^S[j]) \leq \psi$  then
8       if  $i$  is  $j$  then
9         continue
10      else
11         $index[i] \leftarrow index[i] + \{j\}$ 
12  $index_{rm} \leftarrow RemoveDuplicateData(index)$ 
13  $K \leftarrow Length(index_{rm})$ 
14 for  $i = 0$  to  $K$  do
15    $N \leftarrow Length(index_{remove}[i])$ 
16    $P^t[i] \leftarrow \frac{\sum_{k=0}^N P^S[index_{rm}[i][k]]}{N}$ 
17   for  $j = 0$  to  $N$  do
18      $P^{new}[index_{rm}[i][j]] \leftarrow P^t[j]$ 
19 #Computational cost matrix V:
20 for  $i = 0$  to  $K$  do
21   for  $j = 0$  to  $K$  do
22     if  $i$  is  $j$  then
23       continue
24     else
25       calculate  $V_{[i][j]}$  by Eq.(2) with  $P^t[i]$ ,  $P^t[j]$  and  $P^{new}$ 
26 #The TSP solution:
27  $D_s = []$ 
28 for  $k = 0$  to  $K$  do
29    $N \leftarrow Length(index_{rm}[k])$ 
30   if  $N > 1$  then
31     continue
32   else
33      $p_{init} \leftarrow P^t[k]$ 
34      $\bar{P}_{/k} \leftarrow P^t - \{P^t[k]\}$ 
35     get shortest closed polygons as  $D_s[i]$  by Eq.(3) with  $V$ ,  $\bar{P}_{/k}$  and  $p_{init}$ 
36  $P_{result} \leftarrow RemoveDuplicateSurface(D_s)$ 
```

TSP algorithm: The problem of surfaces segmentation is equivalent to find all closed polygons without overlap in $G(P^t, V)$, and we can use the TSP[32] method to find the closed polygons. Firstly, we set two-line point as an initial point p_{init} (28 to 33 line in Algorithm1) and remove the initial point in P^t as \bar{P} (34 line in Algorithm1). Then the path with the least cost to return to p_{init} in \bar{P} calculated by Eq.3 is the segmented surface. Finally, we use each point which belongs to two-line points as initial point to get the surfaces and remove the duplicate surfaces(28 to 36 line in Algorithm1).

$$F(p_{init}, G(\bar{P}, V)) = \min F(p_k, G(\bar{P}/k, V)) + V_{init,k} \quad \text{s.t.} \begin{cases} p_{init} \in P^t \\ p_k \in \bar{P} \\ \bar{P}/k = \bar{P} - \{p_k\} \\ \sum_{i=0}^{|P^t|} V_{i,j} \leq 3 \\ \sum_{j=0}^{|P^t|} V_{i,j} \leq 3 \end{cases} \quad (3)$$

In Eq.3, $\bar{P}/k = \bar{P} - \{p_k\}$ is the unsearched point set. $\sum_{i=0}^{|P^t|} V_{i,j} \leq 3$ and $\sum_{j=0}^{|P^t|} V_{i,j} \leq 3$ are the conditions that any point in P^t is connected with other points at most 3 times. And when $V_{k,init} = 1$, the $F(p_k, G(\bar{P}, V))$ ends up and the path is a closed polygon. Finally the path with least cost is a surface of the carton.

3.4. Contour reconstruction algorithm

Theoretical analysis: As we know, for an incomplete contour of surface, it can be obtained by occlusion and truncation with many parallelograms, and for parallelograms with too large scale, it is easy to cause the synthesized image to be not realistic. So we add an additional condition with smallest area when we construct a complete contour. Assuming that the incomplete contour of the surface is X , and the parallelogram contour is Y . The goal is to find a optimal parallelogram Y^* with our conditions in contour sets Ω^{R^2} , as shown in Eq.4.

$$Y^* = \arg \max_{Y \in \Omega^{R^2}} P(Y|X) \quad \text{s.t.} \begin{cases} S_{Y^*} = \min S_Y \\ K_A = K_C \ \& \ K_B = K_D \end{cases} \quad (4)$$

In Eq.4, $S_{Y^*} = \min S_Y$ represents the complete contour with the smallest area. K is the slope of the line, $A, B, C,$ and D are the edge of parallelogram. $K_A = K_C$ and $K_B = K_D$ are the conditions of the parallelogram rule to construct a parallelogram.

Because of the perspective transformation principle, some surfaces with complete contours in X may not satisfy the parallelogram contour. In order to maintain the perspective transformation relationship of the complete contour as much as possible, we compare the area of the original complete contour(it is assumed that the contour represented by 4 points is a complete contour) with the area of the parallelogram constructed by Eq.4 to get the final contour. The final contour Y_{final} is calculated as shown in Eq.5.

$$Y_{final} = \begin{cases} y, \\ Y^*, \end{cases} \quad \text{s.t.} \begin{cases} \gamma < \frac{area(y)}{area(Y^*)} \\ len(y) = 4 \\ others \end{cases} \quad (5)$$

In Eq.5, y represents the original contour. The $len(y) = 4$ is the condition that the original contour is represented by 4 points. $area(*)$ is the area of each contour. γ is the hyperparameter to decide the final contour and $\gamma = 2/3$ is used in our experiments .

Parallelogram reconstruction: As we all known, the parallelograms satisfy the convex polygon condition(as shown in definition2). So during constructing a parallelogram, we select a line $A(ap_{i_x} + bp_{i_y} + c = 0)$ from the edge of incomplete contour as the constructed line(as shown in definition3). And let us denote by $P_{surface} = \{p_0, p_1, \dots, p_n\}$ the incomplete contour. When A and it's adjacent edge B in $P_{surface}$ both satisfy the convex polygon condition, we construct a parallelogram with A and B . Firstly, we get the point P_A with farthest distance to A , and P_B with farthest distance to B in $P_{surface}$. Then we calculate the slope of A and B as K_A, K_B and construct the other edges(C and D) of parallelogram with (K_A, P_A) and (K_B, P_B) (22 to 25 line in algorithm2). Finally, we calculate the point of intersection of each edge in A, B, C, D to get the parallelogram(26 to 29 line in algorithm2).

Definition 2. *Convex polygon condition: All points in the parallelogram must be on the side of any edge.*

Definition 3. *Constructed line: when constructing a parallelogram, the selected line which is the edge of the parallelogram is a constructed line. It is judged by Eq.6 and Eq.7. And when $|\beta|$ equals to $|m - n|$, the selected line is a constructed line.*

$$\beta = \sum_{i=0}^n \beta_i \quad \text{s.t} \quad \begin{cases} p_i \in P_{surface} \\ \beta_i = \begin{cases} 1, & \text{if : } ap_{i_x} + bp_{i_y} + c > 0 \\ 0, & \text{if : } ap_{i_x} + bp_{i_y} + c = 0 \\ -1, & \text{others} \end{cases} \end{cases} \quad (6)$$

$$m = \sum_{i=0}^n g_i \quad \text{s.t} \quad g_i = \begin{cases} 1, & \text{if : } \beta_i = 0 \\ 0, & \text{others} \end{cases} \quad (7)$$

In Eq.6 and Eq.7, m is the number of points in the constructed line. (p_{i_x}, p_{i_y}) is the coordinate of point p_i in $P_{surface}$.

Parallelogram reconstruction strategy: Due to the perspective transformation of imaging, the cartons appear in three kinds of appearance in the image including single visible surface, two visible surfaces and three visible surfaces. The contour reconstruction methods for these three kinds of appearance are as follows:

(1) single visible surface reconstruction: When there is no occlusion as **All** according to the labeling rules, the contour keeps unchanged. When the carton is labeled as **Occlusion**, we select each edge in $P_{surface}$ as the constructed line to construct a parallelogram and we choose the parallelogram with smallest area as the contour of the $P_{surface}$ (as shown in algorithm2).

(2) two visible surfaces: Because there is a common line, when we construct a parallelogram, we only use the common line as constructed line to construct parallelograms for each surface. And we also choose the parallelogram with smallest area as the contour of the $P_{surface}$. Finally, for the parallelogram of each surface, we should adjust it's scale, so that the coordinate of the common line in each surface is equal in image.

(3) three visible surfaces: Because there are two common lines in each surface, when we construct a parallelogram, we use the common lines as constructed line and its adjacent edge to construct a parallelogram for each surface. Finally, for the parallelogram of each surface, we also should adjust it's scale, so that the coordinate of the common line in each surface is equal in image.

Algorithm 2: single visible surface reconstruction

Input: $P_{surface} = \{p_i\}_{i=0}^n$: incomplete contour points; *Label*: label information

Output: the complete contour points of surface: $P_c = \{p_i\}_{i=0}^3$

```
1 Initialize:  $FLAG = False$ : True means the constructed line and it's adjacent edge both
   satisfy the convex condition;  $(A, B, C)$  is the parameters of line  $Ax + By + C = 0$ .
2 if Label is all then
3   |  $P_c \leftarrow P_{surface}$ 
4 else
5   for  $i = 0$  to  $n$  do
6     | calculate the parameters  $(A_1, B_1, C_1)$  of the  $line_1$  with  $P_{surface}[i], P_{surface}[i + 1]$ 
7     | calculate the parameters  $(A_2, B_2, C_2)$  of the  $line_2$  with  $P_{surface}[i + 1], P_{surface}[i + 2]$ 
8     | for  $k = 0$  to  $n$  do
9       |  $\beta_1[k], g_1[k] \leftarrow$  calculated by Eq.(6) and Eq.(7) with  $line_1$  and  $P_{surface}[k]$ 
10      |  $\beta_2[k], g_2[k] \leftarrow$  calculated by Eq.(6) and Eq.(7) with  $line_2$  and  $P_{surface}[k]$ 
11      |  $\beta_{line1} \leftarrow \sum_{i=0}^n \beta_1[i]$ 
12      |  $m_{line1} \leftarrow \sum_{i=0}^n g_1[i]$ 
13      |  $\beta_{line2} \leftarrow \sum_{i=0}^n \beta_2[i]$ 
14      |  $m_{line2} \leftarrow \sum_{i=0}^n g_2[i]$ 
15      | if  $|\beta_{line1}|$  is  $|n - m_{line1}|$  and  $|\beta_{line2}|$  is  $|n - m_{line2}|$  then
16        |  $FLAG \leftarrow True$ 
17      | else
18        |  $FLAG \leftarrow False$ 
19      |  $K_1 \leftarrow \frac{P_{surface}[i]_y - P_{surface}[i+1]_y}{P_{surface}[i]_x - P_{surface}[i+1]_x}$  #slope of line1
20      |  $K_2 \leftarrow \frac{P_{surface}[i+1]_y - P_{surface}[i+2]_y}{P_{surface}[i+1]_x - P_{surface}[i+2]_x}$  #slope of line2
21      | if  $FLAG$  is  $True$  then
22        |  $P_1$  is the point with farthest distance to line1 in  $P_{surface}$ 
23        |  $P_2$  is the point with farthest distance to line2 in  $P_{surface}$ 
24        | calculate the parameters  $(A_3, B_3, C_3)$  of the  $line_3$  with  $K_1$  and  $P_1$ 
25        | calculate the parameters  $(A_4, B_4, C_4)$  of the  $line_4$  with  $K_2$  and  $P_2$ 
26        |  $Point[0] \leftarrow P_{surface}[i + 1]$ 
27        |  $Point[1] \leftarrow CalculatePointofIntersection(line_3, line_2)$ 
28        |  $Point[2] \leftarrow CalculatePointofIntersection(line_3, line_4)$ 
29        |  $Point[3] \leftarrow CalculatePointofIntersection(line_1, line_4)$ 
30        |  $P_{list}[i] \leftarrow Point$ 
31        |  $S[i] \leftarrow area(Point)$ 
32      | else
33        |  $P_{list}[i] \leftarrow Null$ 
34        |  $S[i] \leftarrow Infinity$ 
35      | if  $n$  is not 4 then
36        |  $P_c \leftarrow$  Get the complete contour by Eq.(4) with  $P_{list}$  and  $S$ 
37      | else
38        |  $P_c \leftarrow$  Get the complete contour by Eq.(4) and Eq.(5) with  $P_{list}$  and  $S$ 
```



Figure 5: The example of foreground texture labeling rules. (a) is the labeling rules of the two visible surfaces, we label the instance according to arrow and starting to common line; (b) is the labeling rules of the three visible surfaces, we also label the instance according to arrow. The image in the first row and first column is vertical view; the image in the second row and first column is the front view, and the image in the second row and last column is end view. As we can see in the first row and last column, the combination relationship of the surface is fixed with each other in the carton instance.

3.5. Image synthesis

Foreground texture datasets: We have collected different kinds of cartons which have only one surface as the foreground texture datasets(as shown in Fig.2d). Because the carton is composed of multiple surfaces and each surface has a specific combination relationship(such as the direction of the surface with each other) with each other as shown in Figure 5b. We use the method shown in Figure 5 to label the foreground instance to ensure the true relationship with each other. And we build a subset of data in the foreground texture datasets according to the number of visible surface.

Image synthesis method: During performing the image synthesis algorithm, we use perspective transformation principle to adaptively deform the foreground instance to ensure the linearity of the edges. The coordinates of the foreground instance are $P_{pre} = \{p_i\}_{i=0}^3$, and the coordinates of the reconstructed contour are $P_{back} = \{p_j\}_{j=0}^3$, the perspective principle is as follows:

$$\begin{bmatrix} P_{pre} \\ 1 \end{bmatrix} = M \times \begin{bmatrix} P_{back} \\ 1 \end{bmatrix} = \begin{bmatrix} a_{00} & a_{01} & a_{02} \\ a_{10} & a_{11} & a_{12} \\ a_{20} & a_{21} & a_{22} \end{bmatrix} \begin{bmatrix} P_{back} \\ 1 \end{bmatrix} \quad (8)$$

M can be solved when P_{pre} and P_{back} are fixed. Then, we use M to generate images by Eq.9. In Eq.9, I is the original image from source datasets, I_{pre} is the foreground instance texture from target datasets, I_{back} is the mask of the reconstructed contour, I_x is the mask of the original instance of I and $I_{synthetic}$ is the synthetic image. The \odot represents the image fusion operation [11] as shown in the fifth module in Figure 3. And \oplus represents the pixel-level image merging operation.

$$I_{synthetic} = (M \times I_{pre} \odot I_x) \oplus ((\mathbf{1} - I_x) \odot I) \quad (9)$$

Because the carton is composed of multiple surfaces in the image, the texture from foreground texture datasets needs to be selected according to the relationship of the surface in I . For single visible surface, I_{pre} is randomly selected. And for the two visible surfaces and three visible surfaces, we firstly select the subset of data corresponding to the number of surfaces, then we randomly select the foreground instance textures to generate image.

Subtle pixel artifacts: In the process of image synthesis, because of the brightness difference between I_{pre} and I , there must be some artificial noise in $I_{synthetic}$, such as the subtle pixel artifacts

at the edge of the synthesized instance[11]. In order to reduce the influence of subtle pixel artifacts, we use Gaussian fusion method for foreground texture fusion. And we use the method in Ref.[13] to replace the instance texture with a random noise texture with a probability of 0.2 (as shown in Figure 3) to make the detection model focus only on the object appearance.

4. Experiments

This chapter mainly explores the application of surfaces segmentation algorithms and contour construction algorithms in the field of data expansion. We will verify the effectiveness of our method on the object detectors such as RetinaNet[6] and Faster R-CNN[3]. All experiments are based on PyTorch and conducted on 2 GTX1080Ti.

4.1. Experimental Settings

Datasets: The information of the SCD is shown in Table 1. We sampled 520 images from CPLC as the carton stacking skeleton data and used the method in chapter 3.2 to label them. Finally, we randomly selected 269 single-sided instances, 51 double-sided instances, and 23 three-sided instances from FM as the substitute texture for foreground. In addition, 149 single-sided instances, 27 double-sided instances, and 30 three-sided instances are randomly sampled from ECLC for texture replacement. All experiments take CPLC as base dataset which is split into 3589 images for training and 500 images for testing.

Scene	Train No.	Test No.	Stacked skeleton No.	foreground texture datasets		
				Single sides	Two sides	three sides
CPLC	3589	500	520	0	0	0
ECLC	1722	500	0	149	27	30
FM	0	492	0	269	51	23

Table 1: Data distribution of the SCD datasets in different scenarios and distribution of the texture datasets

Evaluation metric: In this paper, we adopt the same performance measure as the MS COCO Challenge [7] to report the experimental results. This includes the calculation of mean Average Precision (mAP) for a specific value of the IoU threshold to determine true positives and false positives. The main performance measure used in this benchmark is shown by AP, which is averaging mAP across the different value of IoU thresholds, i.e. $\text{IoU} = .5, .6, .7, \dots, .9$.

Implementation details: All experiments are implemented based on PyTorch[34] and MMDetection [35]. We utilize ResNet-18 as backbones in RetinaNet[6]. The backbones are pre-trained on ImageNet. We use a mini-batch of 4 images per GPU during training RetinaNet[6] and Faster R-CNN[3], thus making a total mini-batch of 8 images on 2 GPUs. The synchronized Stochastic Gradient Descent (SGD) is used for model optimization. The weight decay of 0.0001 and the momentum of 0.9 are adopted. A linear scaling rule[36] is carried out to set the learning rate during training (0.005 in RetinaNet and 0.01 in Faster R-CNN). And a linear warm-up strategy is adopted in the first 500 iterations. Except that the learning rate changes linearly with mini-batch, the flip ratio is 0.5 and the image scale is [600, 1000] in all experiments. And other settings are consistent with the default settings of MMDetection[35].

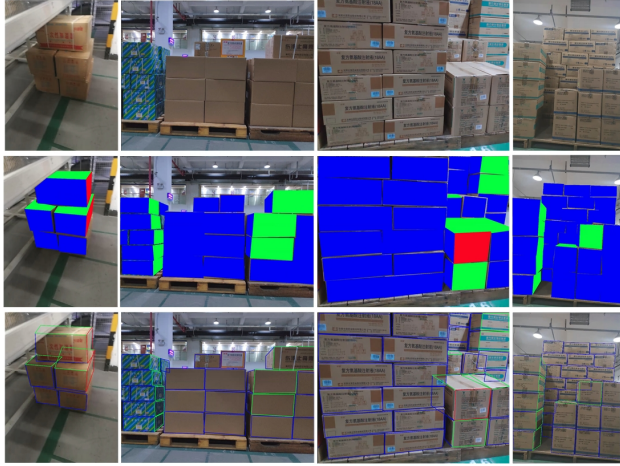


Figure 6: The results of surfaces segmentation algorithm and contour reconstruction algorithm. The first line is the original picture. The second line is the result of surfaces segmentation algorithm when $\psi = 25$. If the carton has one surface, it is represented by blue, the two surfaces are represented by blue and green, and the three surfaces are represented by blue, green, and red for different surfaces. The third row is the result of the contour reconstruction algorithm, and the contour of different colors represent the complete contour.

4.2. Qualitative Analysis

The results of surfaces segmentation algorithm: We select 520 images as the carton stacking skeleton datasets from CPLC and then surfaces segmentation algorithm are conducted to extract the segmentation surfaces of the skeleton (see second row of Fig.6). To search for the best result of the surfaces segmentation algorithm, sampling statistics are employed to achieve the optimal hyperparameter ψ . For each group of ψ , we randomly select 10 pictures for surfaces segmentation algorithm. Then we compute the percentage of incorrectly parameter with the smallest average error. Table 2 reports that the best result is achieved with $\psi = 25$ while Fig.7 show the corresponding visualization.

	1	2	3	4	5	mean
$\psi = 10$	3.52%	2.8%	0	9.41%	8.33%	4.81%
$\psi = 15$	1.41%	2.8%	0	1.34%	5.00%	2.11%
$\psi = 20$	0	0	0	0	0.08%	0.016%
$\psi = 25$	0	0	0	0	0	0

Table 2: Statistics of error rate of the faceted results under different hyperparameters ψ .

The results of contour reconstruction algorithm: Because of the occlusion and truncation, the contours of the instances are incomplete. With the method in Chapter 3.4, we construct the complete contours which are shown in Fig.6. We also use sampling statistics for evaluation to get the optimal value of the γ . For each group of γ , we randomly select 10 pictures from the carton stacking skeleton datasets for surfaces segmentation algorithm, then we perform contour construction. Finally, we compute the percentage of unreasonable samples (the examples that are occluded but not reconstructed by our method, or the examples are reconstructed but unreasonable compared with the original complete contour) in the total instances. Table 3 reports that the smallest average error is achieved when setting γ as $\frac{2}{3}$ while Fig.8a shows the corresponding visualization. The same procedure are conducted in FM to search the optimal value of γ . The

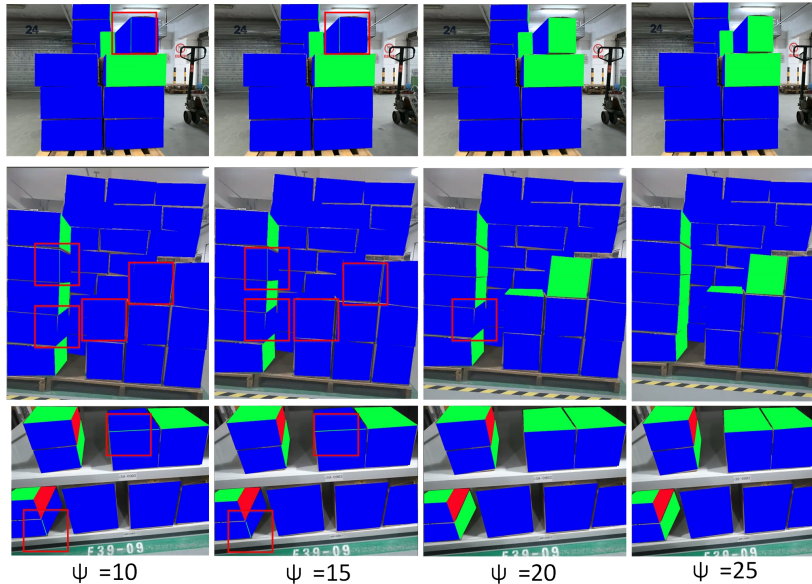


Figure 7: The result of surfaces segmentation algorithm under different hyperparameters ψ . If the carton has one surface, it is represented by blue, the two surfaces are represented by blue and green, and the three surfaces are represented by blue, green, and red for different surface. The red square is the wrong result of the surfaces segmentation algorithm.

generated are mixed with the training sets of CPLC and then fed into RetinaNet for training. As shown in Fig.8b, the fine-tuning detector is used to test data in different scenarios and achieving best performance with $\gamma = \frac{2}{3}$.

	1	2	3	4	5	mean
$\gamma = \frac{1}{4}$	9.86%	10.19%	8.72%	8.24%	10.83%	9.57%
$\gamma = \frac{1}{3}$	9.86%	9.26%	8.72%	8.24%	10.00%	9.22%
$\gamma = \frac{1}{2}$	9.86%	9.26%	8.72%	8.24%	10.00%	9.16%
$\gamma = \frac{2}{3}$	7.04%	8.33%	6.71%	8.24%	9.17%	7.90%
$\gamma = \frac{3}{4}$	7.75%	9.26%	7.38%	8.24%	9.17%	8.36%

Table 3: The ratio of unreasonable contours generated by different values of the γ to the total number of sample instances

Image synthesis: After contour reconstruction, we use the Gaussian fusion method to generate images. In the processing of image synthesis, the instances from foreground instance texture datasets are randomly selected up to the same number of surfaces in the skeleton picture. And then we replace the instance texture in the skeleton picture with the texture from foreground texture datasets. Because of the influence of the subtle pixel artifacts, we use the method in [13] to replace this shown in 9a.

4.3. Main Results

Baselines on carton datasets: To establish baselines, RetinaNet[6] and Faster R-CNN[3] both equipped with ResNet18 are employed to fine-tuning on training set of CPLC and test respectively on 500 images from ECLC and 492 images from FM. The overall results are reported in Table 4 which shows that huge domain shift exists from CPCL to FM and ECLC up to 23% \sim 27.7% in AP.

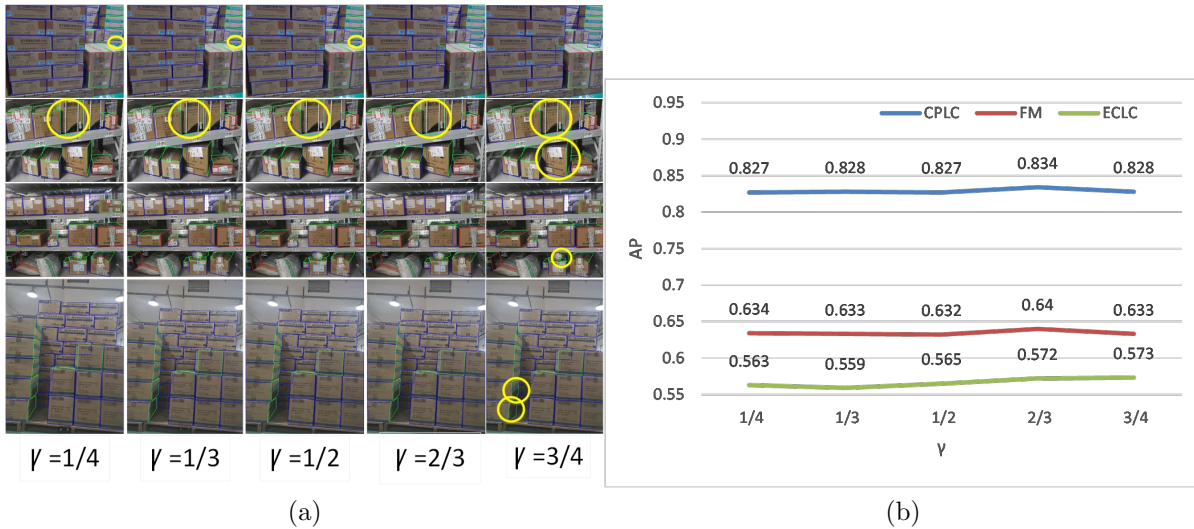


Figure 8: (a) the results of the contour reconstruction under different γ . The yellow ellipse indicates unreasonable contour reconstruction. (b) it is to generate 6000 images for each γ when FM is the foreground texture datasets. Then the generated images are mixed with the train datasets which contains 3589 images in CPLC to train the RetinaNet[6] detection model.

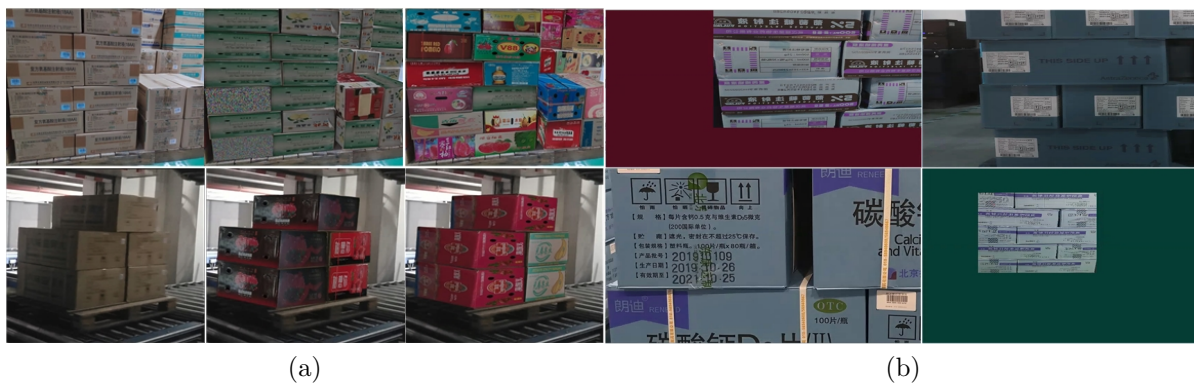


Figure 9: (a) Image synthesis renderings, the first column is the original image and the rest are the generated images. (b) Data augmentation for CPLC with random scaling, random flipping, random cutting etc.

Foreground texture datasets from FM: 343 carton instances with special foreground texture from FM are plugged into 520 skeletons extracted from CPLC. Then we replace the texture of each instance in CPLC skeleton datasets with a random noise texture with a probability of 0.2. Finally, we used the Gaussian fusion method to generate 6000 images and mix with CPLC datasets as CPLC+G_FM. For comparison, we use the data augmentation method to expand the original CPLC dataset (such as random scaling, random flipping, random cutting, etc) to 6000 images (as shown in Figure 9b) as AUG which are subsequently mixed with CPLC to the same scale. The comparative experiments are shown in Table 4.

As shown in Table 4, when RetinaNet and Faster R-CNN are trained on CPLC+G_FM and tested on CPLC, the AP can be improved by 2% and 1.5% compared with training on CPLC. In addition, compared with only training on CPLC+AUG, the performance of our method can improve AP by 0.5% and 0.6%. This demonstrates that our method is better than the traditional data augmentation strategy. And when RetinaNet and Faster-RCNN are tested on FM, the AP increases by 6.5% and 6.8% compared with training on CPLC. When testing on ECLC, the AP

datasets	train No.	model	test	AP	AP_{50}	AP_{80}
Baseline: CPLC	3589		CPLC	0.814	0.970	0.877
			FM	0.575	0.810	0.569
			ECLC	0.546	0.798	0.520
CPLC+AUG	9589	RetinaNet[6]	CPLC	0.829	0.969	0.8895
			FM	0.588	0.812	0.589
			ECLC	0.552	0.791	0.533
CPLC+G_FM	9589		CPLC	0.834	0.973	0.896
			FM	0.640	0.852	0.650
			ECLC	0.572	0.810	0.568
Baseline: CPLC	3589		CPLC	0.837	0.976	0.902
			FM	0.607	0.811	0.624
			ECLC	0.577	0.813	0.580
CPLC+AUG	9589	Faster R-CNN[3]	CPLC	0.846	0.976	0.910
			FM	0.616	0.815	0.625
			ECLC	0.573	0.792	0.573
CPLC+G_FM	9589		CPLC	0.852	0.977	0.914
			FM	0.675	0.855	0.700
			ECLC	0.593	0.806	0.588

Table 4: The performance of the method in this paper to generate FM foreground texture images on the detection model.

also can be improved by 2.6% and 1.6% compared with training on CPLC. This demonstrates that our method can greatly ease the problem of domain shift. Finally, RetinaNet and Faster R-CNN are tested on FM and ECLC, they are compared with training on CPLC+AUG, the performance of our method can improve AP by 5.2% and 5.9% on FM test set and 2% and 2% on ECLC test set. This demonstrates that our method is not only better than the traditional data augmentation strategy for data augmentation, but also can effectively ameliorate the problem of domain shift.

Foreground texture datasets from ECLC: We use the foreground instances in ECLC which contain 206 instances as foreground texture datasets, the skeleton in CPLC as the template datasets. And the parameters of all algorithms are kept the same as before. Finally, we used the Gaussian fusion method to generate 6000 images and mix them with CPLC datasets as CPLC+G_ECLC, the results are shown in Table 5.

It can be seen in Table 5 that the AP of the CPLC+G_ECLC are compared with the baseline on the RetinaNet is improved by 1.7% on CPLC. And the AP of RetinaNet training on CPLC+G_ECLC is improved by 2% on the FM, 4.3% on ECLC compare with training Baseline. At the same time, compared with the CPLC+AUG, the CPLC+G_ECLC has a slightly improvement of only 0.2% on the CPLC, 0.7% on FM. But it is improved by 3.7% on ECLC. In the Faster R-CNN, our method improve by 0.9% on CPLC, 1.7% on FM, and 3.4% on ECLC compare with baseline. Our method outperforms the CPLC+AUG with 0.8% on FM and 3.8% on test sets of CPLC. This further demonstrates that our method is not only better than the traditional data augmentation strategy for data augmentation, but also can effectively solve the problem of domain shift. Because the number of foreground texture datasets from ECLC is smaller than that from FM, it causes the performance of ECLC to be lower than that of FM.

According to the results in Table 4 and 5, our method achieve great successes in both detectors

datasets	train No.	model	test	AP	AP_{50}	AP_{80}
Baseline: CPLC	3589		CPLC	0.814	0.970	0.877
			FM	0.575	0.810	0.569
			ECLC	0.546	0.798	0.520
CPLC+AUG	9589	RetinaNet[6]	CPLC	0.829	0.969	0.8895
			FM	0.588	0.812	0.589
			ECLC	0.552	0.791	0.533
CPLC+G_ECLC	9589		CPLC	0.831	0.972	0.894
			FM	0.595	0.820	0.598
			ECLC	0.589	0.812	0.575
Baseline: CPLC	3589		CPLC	0.837	0.976	0.902
			FM	0.607	0.811	0.624
			ECLC	0.577	0.813	0.580
CPLC+AUG	9589	Faster R-CNN[3]	CPLC	0.846	0.976	0.910
			FM	0.616	0.815	0.625
			ECLC	0.573	0.792	0.573
CPLC+G_ECLC	9589		CPLC	0.846	0.975	0.909
			FM	0.624	0.830	0.635
			ECLC	0.611	0.818	0.627

Table 5: The performance of the method in this paper to generate ECLC foreground texture data on the detection model which compared with data augmentation methods

and different scenarios. The reason is that the method achieves texture feature alignment at the instance level. Assuming that the data generated by our method is the source domain $D_s = \{x_i, y_i\}_{i=0}^N$, the unlabeled data set in the test set is $D_T = \{x_i\}_{i=0}^M$. The object detection problem can be viewed as learning the posterior $P(C, B|I)$, where I is the image representation, B is the bounding-box of an object and $C \in \{1, \dots, K\}$ the category of the object (K being the total number of categories, $k = 1$ in this paper). Let us denote the joint distribution of training samples for object detection as $P(C, B, I)$. Because the conditional probabilities in the source domain and target domain are the same as $P_S(C, B|I) = P_T(C, B|I)$. And as we all know, $P_S(I) \neq P_T(I)$, in order to make the source domain and target domain have the same or similar joint probability distribution, the image-level feature alignment is required to make $P_S(I) \approx P_T(I)$. The method in this paper forces $P_S(I) \approx P_T(I)$ from foreground instance texture.

4.4. Ablation Studies

The influence of the probability for RetinaNet that the noise texture is the foreground texture: To explore the impact of random noise for the detectors, we use the foreground texture datasets in FM as a benchmark to generate 3589 images under different probabilities of random noise to train the RetinaNet[6] and test on the CPLC, FM, and ECLC test sets. According to the results in Figure 10, the performance of the model is the best on CPLC and ECLC test sets when the probability of the random noise is 0.2, which means that the random noise can effectively improve the stability of the model, and it can effectively suppress the influence of artificial noise on the model and make the detectors focus only on the object appearance.

The influence of the amount of generated images for detectors: To explore the influence of the number of the generated images for the detectors, we use FM as the foreground instance

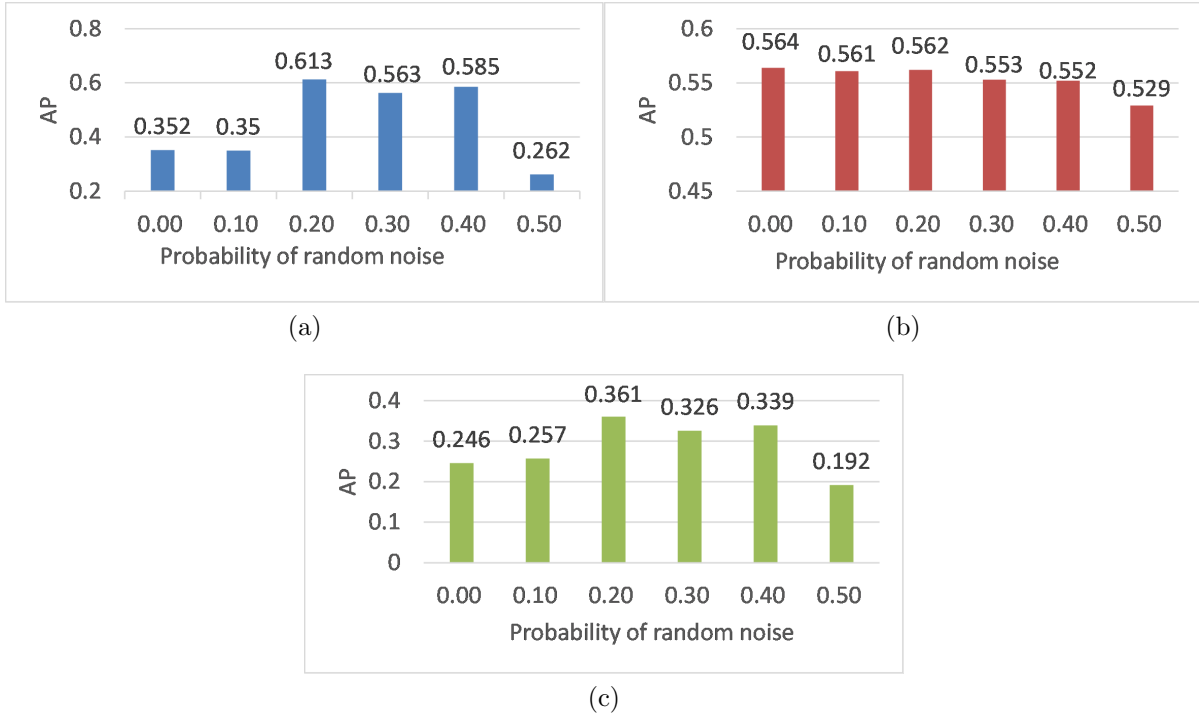


Figure 10: The influence of the probability for RetinaNet that the noise texture is the foreground instance texture. We use FM as the foreground texture datasets to generate 3589 images and directly train the RetinaNet[6] model. (a) is the result of testing on CPLC,(b) is the result of testing on FM,(c) is the result of testing on ECLC. As shown in the figure, the best probability is 0.2 .

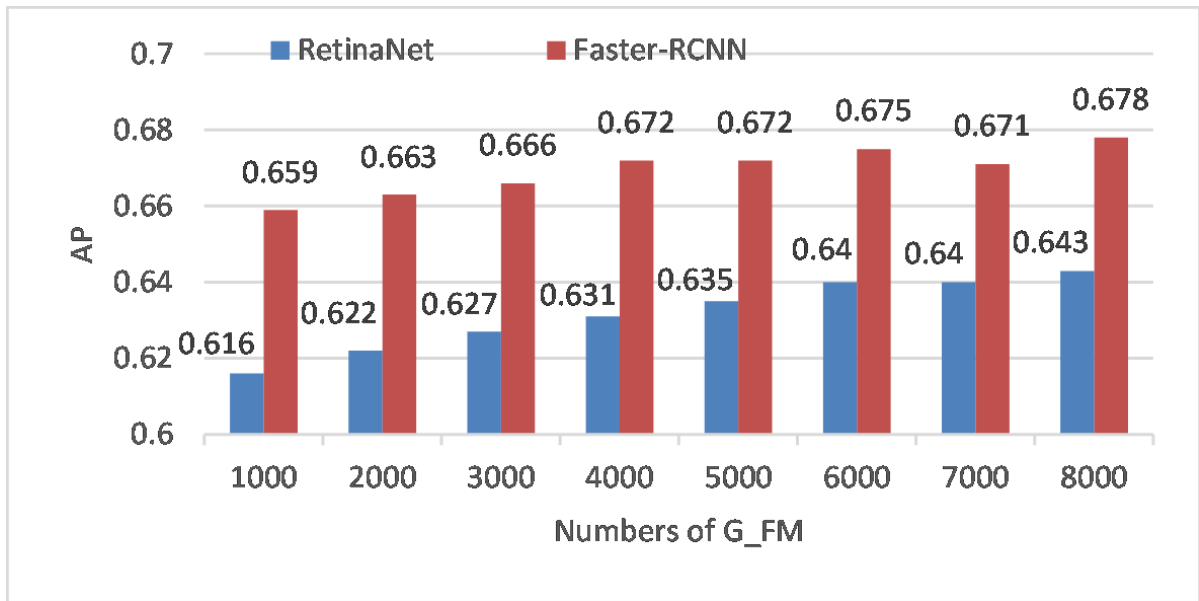


Figure 11: The influence of the amount of generated images for detection model. FM is the foreground texture datasets to generate different numbers of training sets as G_FM and mix them with the CPLC train sets and test them on the FM test sets.

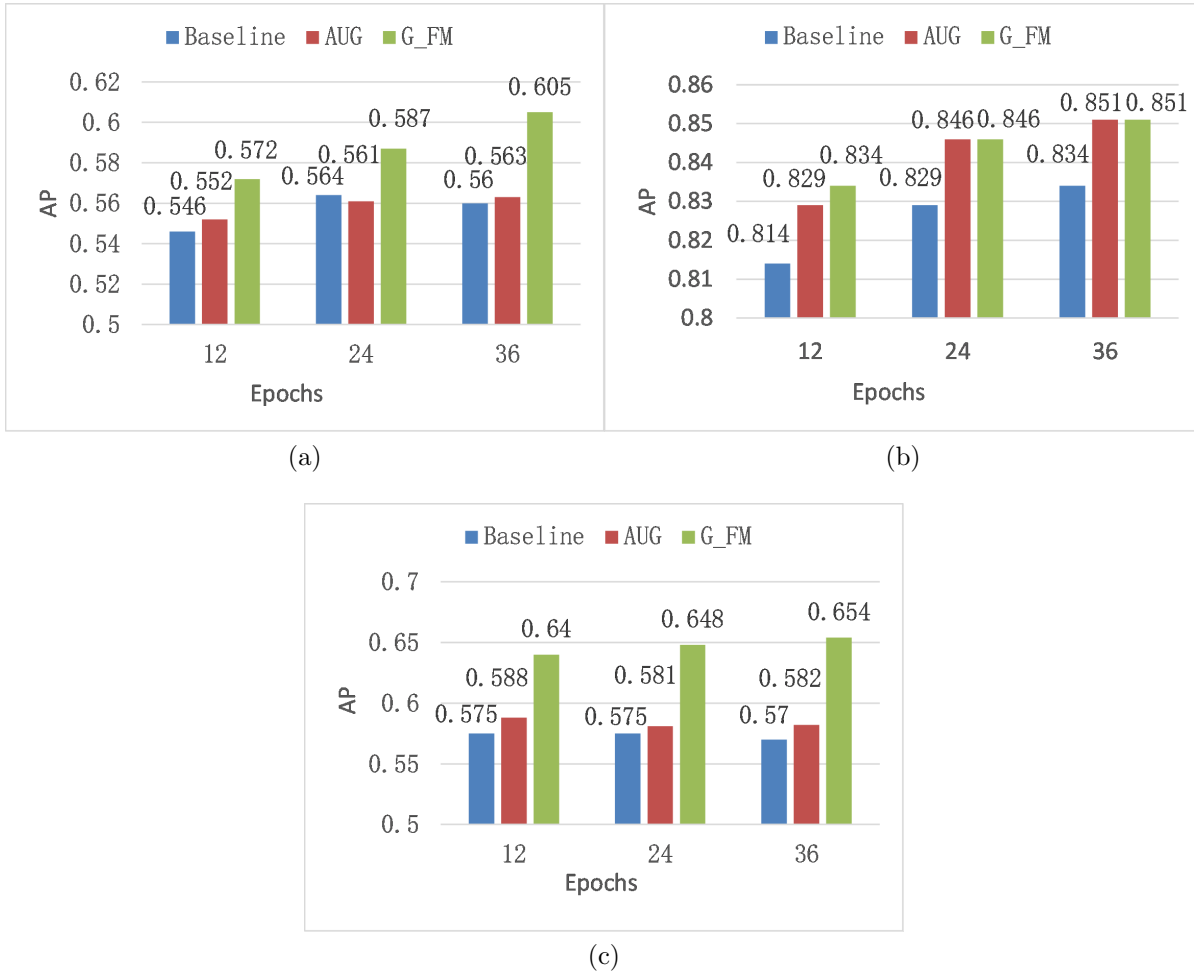


Figure 12: The influence of epochs in RetinaNet [6],(a) the result of testing on the ECLC test sets,(b) the result of testing on the CPLC test sets,(c) the result of testing on FM test sets. It can be seen from the figure that our method has the best performance in all test sets, and secondly, the performance of our method has the best improved on the FM test sets.

texture datasets and set the random noise probability as 0.2 to generate different numbers of images, then mix them with the CPLC training datasets to train the RetinaNet [6] and Faster R-CNN [3]. Finally, we test them on FM. As shown in Figure 11, the performance of the models increases as the number of the generated images increases. Compared with the baseline in Table 4, the performance of our methods is improved by 6.8% on RetinaNet and 7.1% on Faster-RCNN when the number of generated images is 8000. However, the performance of the RetinaNet and Faster R-CNN increase slowly when the number of the generated images exceeds 6000. Because the influence of subtle pixel artifacts, our method is saturated when the number of generated images is more than 6000.

The influence of training epochs in RetinaNet: We conduct experiments with respect to the number of training epochs on the RetinaNet(as shown in Figure 12). We mix G_FM datasets in Chapter 4.3 with CPLC datasets as the training datasets named CPLC+G_FM, and test on CPLC, FM, ECLC test sets. The performance of our method on FM test set compared with the CPLC datasets is improved to 8.4% when the number of training epochs is 36. And it proves that our method can ease the problem of domain shift. Because the number of epochs increases, the

model learns more basic features.

5. Conclusions

We propose a simple method based on the SCD to synthesize annotated images for object detection. And our method is not only better than the traditional data augmentation strategy for data augmentation, but also can effectively solve the problem of domain shift. The analysis of qualitative experiments and quantitative statistical experiments shows that the surfaces segmentation algorithm can effectively decompose the surfaces of the cartons. And our contour reconstruction algorithm can effectively reconstruct a complete contour for the incomplete contour of the carton instance.

Our method is not limited to the application of the carton data set. Our method is also applicable to the task of any rectangular instance. In the future, we will explore the application of this framework in one-shot learning and simpler surfaces segmentation algorithms. Secondly, we will explore how to reduce the harm of the subtle pixel artifacts to the model, and finally, we will explore the brightness adaptive foreground and background fusion.

6. Acknowledgements

This research did not receive any specific grant from funding agencies in the public, commercial, or not-for-profit sectors.

References

- [1] K. He, X. Zhang, S. Ren, J. Sun, Deep residual learning for image recognition, in: Proceedings of the IEEE conference on computer vision and pattern recognition, 2016, pp. 770–778.
- [2] J. Long, E. Shelhamer, T. Darrell, Fully convolutional networks for semantic segmentation, in: Proceedings of the IEEE conference on computer vision and pattern recognition, 2015, pp. 3431–3440.
- [3] S. Ren, K. He, R. Girshick, J. Sun, Faster r-cnn: Towards real-time object detection with region proposal networks, *IEEE transactions on pattern analysis and machine intelligence* 39 (2016) 1137–1149.
- [4] A. Bochkovskiy, C.-Y. Wang, H.-Y. M. Liao, Yolov4: Optimal speed and accuracy of object detection, *arXiv preprint arXiv:2004.10934* (2020).
- [5] W. Liu, D. Anguelov, D. Erhan, C. Szegedy, S. Reed, C.-Y. Fu, A. C. Berg, Ssd: Single shot multibox detector, in: *European conference on computer vision*, Springer, 2016, pp. 21–37.
- [6] T.-Y. Lin, P. Goyal, R. Girshick, K. He, P. Dollár, Focal loss for dense object detection, in: *Proceedings of the IEEE international conference on computer vision*, 2017, pp. 2980–2988.
- [7] T.-Y. Lin, M. Maire, S. Belongie, J. Hays, P. Perona, D. Ramanan, P. Dollár, C. L. Zitnick, Microsoft coco: Common objects in context, in: *European conference on computer vision*, Springer, 2014, pp. 740–755.

- [8] M. Cordts, M. Omran, S. Ramos, T. Rehfeld, M. Enzweiler, R. Benenson, U. Franke, S. Roth, B. Schiele, The cityscapes dataset for semantic urban scene understanding, in: Proceedings of the IEEE conference on computer vision and pattern recognition, 2016, pp. 3213–3223.
- [9] O. Russakovsky, J. Deng, H. Su, J. Krause, S. Satheesh, S. Ma, Z. Huang, A. Karpathy, A. Khosla, M. Bernstein, et al., Imagenet large scale visual recognition challenge, *International journal of computer vision* 115 (2015) 211–252.
- [10] J. Yang, S. Wu, L. Gou, H. Yu, C. Lin, J. Wang, M. Li, X. Li, Scd: A stacked carton dataset for detection and segmentation, *arXiv preprint arXiv:2102.12808* (2021).
- [11] D. Dwibedi, I. Misra, M. Hebert, Cut, paste and learn: Surprisingly easy synthesis for instance detection, in: Proceedings of the IEEE International Conference on Computer Vision, 2017, pp. 1301–1310.
- [12] S. Liu, H. Guo, J.-G. Hu, X. Zhao, C. Zhao, T. Wang, Y. Zhu, J. Wang, M. Tang, A novel data augmentation scheme for pedestrian detection with attribute preserving gan, *Neurocomputing* (2020).
- [13] S. Tripathi, S. Chandra, A. Agrawal, A. Tyagi, J. M. Rehg, V. Chari, Learning to generate synthetic data via compositing, in: Proceedings of the IEEE Conference on Computer Vision and Pattern Recognition, 2019, pp. 461–470.
- [14] S. Liu, D. Huang, et al., Receptive field block net for accurate and fast object detection, in: Proceedings of the European Conference on Computer Vision (ECCV), 2018, pp. 385–400.
- [15] S. Wu, X. Li, Iou-balanced loss functions for single-stage object detection, *arXiv preprint arXiv:1908.05641* (2019).
- [16] R. Girshick, J. Donahue, T. Darrell, J. Malik, Rich feature hierarchies for accurate object detection and semantic segmentation, in: Proceedings of the IEEE conference on computer vision and pattern recognition, 2014, pp. 580–587.
- [17] T.-Y. Lin, P. Dollár, R. Girshick, K. He, B. Hariharan, S. Belongie, Feature pyramid networks for object detection, in: Proceedings of the IEEE conference on computer vision and pattern recognition, 2017, pp. 2117–2125.
- [18] Z. Cai, N. Vasconcelos, Cascade r-cnn: Delving into high quality object detection, in: Proceedings of the IEEE conference on computer vision and pattern recognition, 2018, pp. 6154–6162.
- [19] J. Pang, K. Chen, J. Shi, H. Feng, W. Ouyang, D. Lin, Libra r-cnn: Towards balanced learning for object detection, in: Proceedings of the IEEE/CVF Conference on Computer Vision and Pattern Recognition, 2019, pp. 821–830.
- [20] K. He, G. Gkioxari, P. Dollár, R. Girshick, Mask r-cnn, in: Proceedings of the IEEE international conference on computer vision, 2017, pp. 2961–2969.
- [21] J. Redmon, S. Divvala, R. Girshick, A. Farhadi, You only look once: Unified, real-time object detection, in: Proceedings of the IEEE conference on computer vision and pattern recognition, 2016, pp. 779–788.

- [22] M. Tan, Q. V. Le, Efficientnet: Rethinking model scaling for convolutional neural networks, arXiv preprint arXiv:1905.11946 (2019).
- [23] A. Krizhevsky, I. Sutskever, G. E. Hinton, Imagenet classification with deep convolutional neural networks, *Communications of the ACM* 60 (2017) 84–90.
- [24] C. Szegedy, W. Liu, Y. Jia, P. Sermanet, S. Reed, D. Anguelov, D. Erhan, V. Vanhoucke, A. Rabinovich, Going deeper with convolutions, in: *Proceedings of the IEEE conference on computer vision and pattern recognition*, 2015, pp. 1–9.
- [25] E. D. Cubuk, B. Zoph, D. Mane, V. Vasudevan, Q. V. Le, Autoaugment: Learning augmentation policies from data, arXiv preprint arXiv:1805.09501 (2018).
- [26] E. D. Cubuk, B. Zoph, J. Shlens, Q. V. Le, Randaugment: Practical automated data augmentation with a reduced search space, in: *Proceedings of the IEEE/CVF Conference on Computer Vision and Pattern Recognition Workshops*, 2020, pp. 702–703.
- [27] G. Ghiasi, Y. Cui, A. Srinivas, R. Qian, T.-Y. Lin, E. D. Cubuk, Q. V. Le, B. Zoph, Simple copy-paste is a strong data augmentation method for instance segmentation, arXiv preprint arXiv:2012.07177 (2020).
- [28] N. McLaughlin, J. M. Del Rincon, P. Miller, Data-augmentation for reducing dataset bias in person re-identification, in: *2015 12th IEEE International conference on advanced video and signal based surveillance (AVSS)*, IEEE, 2015, pp. 1–6.
- [29] G. Georgakis, A. Mousavian, A. C. Berg, J. Kosecka, Synthesizing training data for object detection in indoor scenes, arXiv preprint arXiv:1702.07836 (2017).
- [30] J.-Y. Zhu, T. Park, P. Isola, A. A. Efros, Unpaired image-to-image translation using cycle-consistent adversarial networks, in: *Proceedings of the IEEE international conference on computer vision*, 2017, pp. 2223–2232.
- [31] A. Gupta, A. Vedaldi, A. Zisserman, Synthetic data for text localisation in natural images, in: *Proceedings of the IEEE conference on computer vision and pattern recognition*, 2016, pp. 2315–2324.
- [32] K. L. Hoffman, M. Padberg, G. Rinaldi, et al., Traveling salesman problem, *Encyclopedia of operations research and management science* 1 (2013) 1573–1578.
- [33] B. C. Russell, A. Torralba, K. P. Murphy, W. T. Freeman, Labelme: a database and web-based tool for image annotation, *International journal of computer vision* 77 (2008) 157–173.
- [34] A. Paszke, S. Gross, F. Massa, A. Lerer, J. Bradbury, G. Chanan, T. Killeen, Z. Lin, N. Gimelshein, L. Antiga, et al., Pytorch: An imperative style, high-performance deep learning library, arXiv preprint arXiv:1912.01703 (2019).
- [35] K. Chen, J. Wang, J. Pang, Y. Cao, Y. Xiong, X. Li, S. Sun, W. Feng, Z. Liu, J. Xu, et al., Mmdetection: Open mmlab detection toolbox and benchmark, arXiv preprint arXiv:1906.07155 (2019).
- [36] P. Goyal, P. Dollár, R. Girshick, P. Noordhuis, L. Wesolowski, A. Kyrola, A. Tulloch, Y. Jia, K. He, Accurate, large minibatch sgd: Training imagenet in 1 hour, arXiv preprint arXiv:1706.02677 (2017).